





# Bandwidth Optimization for Mach–Zehnder Polymer/Sol–Gel Modulators

Yasufumi Enami , Senior Member, OSA, Atsushi Seki, Shin Masuda , Senior Member, IEEE, Tomoki Joichi , Jingdong Luo , and Alex K-Y. Jen, Fellow, IEEE, Fellow, OSA

**Abstract**—We demonstrate that the electro-optic (EO) modulation response linearly decreases (dB scale) with respect to the modulating frequency, with an extremely small drop of less than 2 dB, up to a limit of 67 GHz, as measured by an optical component analyzer. The measured bandwidth of the EO response is wider than 67 GHz and was extrapolated to 120 GHz. This study demonstrates a new optimized broadband optical modulator with low half-wave voltage and low optical loss. The dielectric constant of each material in the modulator is accurately measured by comparing the electrical transmission and reflection parameters for the radio frequency (RF) high-speed coplanar electrode deposited on each layer with theoretically obtained values. The electrical transmission bandwidth for the optimized RF electrode is measured up to a limit of 110 GHz by a vector network analyzer and then extrapolated to a 6-dB bandwidth of 130 GHz based on the experimental parameters. The product of the half-wave voltage and electrode length is 1.8 V·cm for dual-drive operation. The in-device EO coefficient is 160 pm/V at 1.55  $\mu\text{m}$ . The product of the half-wave voltage and loss is 10.8 V·dB.

**Index Terms**—Electro-optics, hybrid waveguide modulators, integrated optics devices, optical modulators, polymer active device, sol-gel silica waveguide, ultra-broadband modulators, waveguide modulators.

## I. INTRODUCTION

A BROADBAND optical modulator is a key component for fiber optic communications and optical interconnections and is used for ethernet and optical transceivers owing to its high optical transmission speed of 100 Gbit/s. Next-generation optical transceivers aim to achieve a data transmission speed in the range of 200–400 Gbit/s, which requires high-speed modulators and the corresponding test equipment to be equipped with these modulators for mass production. Specifically, electro-optic

Manuscript received January 20, 2018; revised May 28, 2018 and July 12, 2018; accepted July 25, 2018. Date of publication July 27, 2018; date of current version August 16, 2018. The work of Y. Enami was supported by the Ministry of Internal Affairs and Communications (MIC/SCOPE #171509001). (Corresponding author: Yasufumi Enami.)

Y. Enami is with the Graduate School of Engineering, Optoelectronic Engineering, Kochi University of Technology, Kochi 782-8502, Japan (e-mail: yenami@optics.arizona.edu).

A. Seki, S. Masuda, and T. Joichi are with Advantest Laboratory Ltd., Sendai 989-3124, Japan (e-mail: atsushi.seki@advantest.com; shin.masuda@advantest.com; tomoki.joichi@advantest.com).

J. Luo is with the Department of Chemistry, City University of Hong Kong, Kowloon, Hong Kong, SAR (e-mail: jingdluo@cityu.edu.hk).

A. K-Y. Jen is with the Department of Materials Science and Engineering, University of Washington, Seattle, WA 98198 USA, and also with the City University of Hong Kong, Kowloon, Hong Kong (e-mail: ajen@uw.edu).

Color versions of one or more of the figures in this paper are available online at <http://ieeexplore.ieee.org>.

Digital Object Identifier 10.1109/JLT.2018.2860924

(EO) modulators driven at low voltage are thought to be the most important optical devices in test equipment because when the optical modulator is directly driven by a high-frequency radio frequency (RF) circuit in the test equipment, the test equipment does not need an additional high-frequency RF amplifier circuit. This is advantageous as it enables compact and inexpensive test equipment without a high-speed RF circuit. For example, an epitaxially grown lanthanum-modified lead zirconate titanate modulator [1] has been employed in test equipment [2]. For this purpose, the bandwidth of the Mach-Zehnder (MZ) optical modulators in the test equipment must be extended to more than 100 GHz with a low half-wave voltage ( $V_\pi$ ). Current research focuses on Si modulators, as they are inexpensive and suitable for the high-volume production of photonic integrated circuits in a complementary metal oxide semiconductor (CMOS) platform. Si modulators possess a typical bandwidth in the range of 30–35 GHz [3], [4], with a theoretical limit of 40 GHz [5]. Previous studies have demonstrated modulation speeds in the range of 40–50 Gbit/s [6]–[9]. In addition, the range of values for the product of  $V_\pi$  and the electrode length ( $L$ ), i.e.,  $V_\pi L$ , corresponds to 1–2 V·cm for Si modulators [3], [10], [11]. The optical loss of modulators is also important when several modulators are employed in integrated circuits and their test equipment in the form of cascade or parallel connections. The figure of merit  $V_\pi \text{Loss}$  [12] ( $= V_\pi L [\text{V} \cdot \text{cm}] \times \text{Loss} [\text{dB}] / L [\text{cm}]$ ) of Si modulators typically corresponds to 27–42 V·dB [3], [8], [9], [11], with the minimum value corresponding to 6.7 V·dB [10]. InP electro-absorption (EA) MZ modulators have been reported to exhibit a bandwidth of 67 GHz for optical modulation (3-dB reduction) by using a lightwave component analyzer (LCA) and an extrapolated bandwidth of 74 GHz with a  $V_\pi L$  of 0.022 V·cm and a  $V_\pi \text{Loss}$  of 52 V·dB [13]. Furthermore, MZ InP modulators have been reported to exhibit a bandwidth of 67 GHz and a  $V_\pi$  of 2 V [14].

The bandwidth of the optical modulation is usually measured using an LCA, which is a vector network analyzer (VNA) combined with a high-speed photodetector, in order to directly measure the bandwidth of the optically modulated signal detected on the photodetector. However, optical modulation bandwidths for frequencies above 67 GHz have not been measured due to limitations in the response of the high-speed photodetector in commercially available LCAs. The VNA analyzes the amplitude of the RF signal, and the LCA analyzes the optical signal power on the photodetector after the RF signal is converted to optical power, which is proportional to the squared

amplitude of the optical signal. Therefore, the bandwidth of a 6-dB reduction in the RF signal on the VNA corresponds to that of a 3-dB reduction in the optical signal on the LCA.

The Pockels (EO) effect is attractive for broadband modulators because the dependence of  $V_\pi$  on the operating speed of a Pockels modulator is usually less than that of a non-Pockels modulator (e.g., Si modulators). The RF response of a Pockels modulator is considerably faster than that of a Si modulator. Furthermore, LiNbO<sub>3</sub> modulators are used for long-haul optical communications, with an EO coefficient of 30 pm/V and a bandwidth of 40 GHz. Many reports have measured the optical modulation bandwidth of LiNbO<sub>3</sub> modulators [15]–[20]. The dispersion of the refractive index between the optical frequency and the milliwave frequency corresponds to 3.1 (e.g.,  $n_{opt} = 2.2$ ,  $n_{mw} = 5.3$ ) [15], which results in a limited optical modulation bandwidth (e.g., 43 GHz cm) because of a phase velocity mismatch (walk-off) in the modulator, even though the experimental RF transmission parameter  $S_{21}$  is wider than the bandwidth of the phase velocity mismatch.

The measurement of the optical response has been directly demonstrated using the commercially available LCA up to 67 GHz. When the optical modulators have wider bandwidth of more than 67 GHz, there is another indirect method to measure the bandwidth of the optical response using modulation efficiency (comparing the power in the lower sidebands to the optical reference power and the RF input power) on an optical spectrum analyzer (OSA). The LiNbO<sub>3</sub> modulator demonstrates a  $V_\pi L$  of 17 V-cm at DC frequency [16], [17]. In 1998, K. Noguchi *et al.* determined the bandwidth of the electrical transmission  $S_{21}$  to be approximately 30 and 70 GHz (6-dB reduction) for LiNbO<sub>3</sub> modulators with 3-cm- and 2-cm-long traveling wave RF electrode, respectively, by using a VNA [18]. They also measured an optical modulation bandwidth of 30–45 GHz (3-dB reduction) for the modulator with 3-cm-long RF electrode, using an LCA, and a modulation efficiency bandwidth of 105 GHz (3-dB reduction) for the modulator with 2-cm-long RF electrode, using an optical spectrum analyzer (OSA) [18]. Other reports have also noted the relationship between  $V_\pi$  and the modulation efficiency from low frequency to 20 GHz using a LiNbO<sub>3</sub> modulator [19], [20]. The measurement of the modulation efficiency can be useful to indicate an increase in  $V_\pi$  at higher frequencies of up to 110 GHz [16] and 170 GHz [17]. The LiNbO<sub>3</sub> modulators demonstrated the bandwidth of the modulation efficiency of >170 GHz [17] based on the measurement on the OSA. The modulation efficiency bandwidth of >170 GHz for an EO polymer/gold (Au) plasmon waveguide modulator was determined using an OSA [21]. These reports were excellent to demonstrate the bandwidth of more than 67 GHz.

EO polymer modulators have the advantages of low half-wave voltage – as a result of its high EO coefficient, which is also important for high-speed EO modulation because the lower driving voltage is suitable for compatibility with CMOS – and lower cost for the electronics at the high frequency of more than 60 GHz. Hybrid EO polymer/sol-gel silica MZ waveguide modulators [22] exhibit the lowest  $V_\pi$  of 0.65 V (in-device EO coefficient of 142 pm/V) for a 2.4-cm-long dual-drive electrode

[23] and an optical propagation loss of 5 dB/cm, which corresponds to  $V_\pi L = 1.56$  V-cm and  $V_\pi Loss = 7.8$  V-dB. The EO polymer is efficiently poled on the sol-gel silica cladding because the electrical conductivity of the sol-gel silica exceeds that of the EO polymer by more than one order of magnitude [22]. Recently, Enami *et al.* reported a wider bandwidth for hybrid modulators, in which the electrical transmission of the RF electrode was measured up to a frequency of 50 GHz [24].

EO polymer modulators are a type of Pockels modulators and are usually composed of dielectric materials, which have advantageous bandwidths because of their low refractive index dispersion. All-polymer phase modulators enable a broadband phase modulation rate exceeding 100 GHz [25]. A heterodyne detection system exhibited a bandwidth (3-dB reduction) of 74–113 GHz via beating between the optically modulated light signal from the phase modulator and another laser source to down convert the high-frequency optical phase-modulated amplitude signal ( $\sim 100$  GHz) to a low-frequency signal ( $\sim 3$  GHz). An all-polymer MZ modulator also exhibited a bandwidth of the electrical transmission  $S_{21}$  of 100 GHz [26] using a VNA. A previous study demonstrated EO polymer/Si slot waveguide modulators [27]–[29]. EO polymer/TiO<sub>2</sub> multilayer slot waveguide modulators consisting of all-dielectric materials were demonstrated for the first time [30], [31], and a wide bandwidth exceeding 100 GHz was theoretically realized [32]. When the electrode length is reduced to the range of 1 cm, broadband EO modulation exceeding 100 GHz is realized with reasonably low  $V_\pi$ . Here, we present the bandwidth of hybrid EO polymer/sol-gel silica MZ waveguide modulators without a significant decrease in either the electrical transmission or the EO response, which enables high-speed and low-voltage modulation. The conductivities and dielectric constants of the sol-gel silica and EO polymer materials were carefully measured to design MZ modulators with wider bandwidths.

## II. MATERIALS AND EXPERIMENTAL METHOD

Broadband hybrid EO polymer/sol-gel silica waveguide modulators have a single RF input on the top of the waveguide, as shown in Fig. 1. We fabricate two broadband optical modulators. One has the RF electrode length of 1 cm and another has that of 5 mm with same device structure. The long-term stability of  $V_\pi$  is examined by using a previously fabricated modulator. An Au lower ground electrode underneath the sol-gel silica cladding was connected with Au electrode pads fabricated on the modulator surface. The Au top RF traveling-wave electrode and the Au electrode pads via the lower ground electrode were set in a coplanar position such that they could be connected with high-frequency probes or connectors. The top RF electrode covered one of MZ waveguide arms in the demonstration. The output RF traveling wave was also designed and set in the coplanar position such that it could be terminated with a terminator of 50  $\Omega$ . A 2- $\mu$ m-thick Au lower ground electrode was fabricated using a liftoff process and an Au electroplating technique. A 12.5-nm-thick Ti and 100-nm-thick Au seed multilayer was sputtered on a 6- $\mu$ m-thick thermal oxide SiO<sub>2</sub>/Si substrate as a seed layer for a consecutive electroplating process for the Au lower electrode.

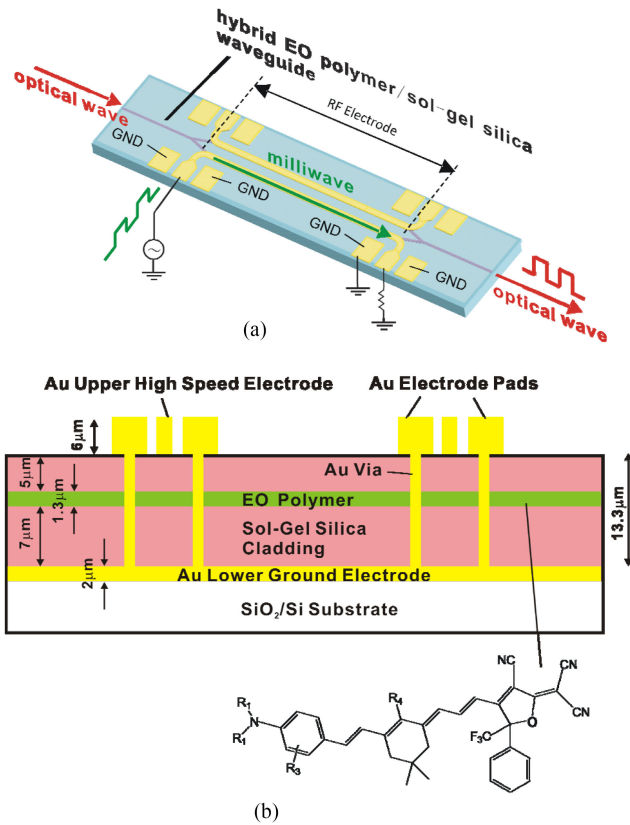


Fig. 1. Schematic of a high-speed hybrid EO polymer/sol-gel silica waveguide modulator: (a) top view and (b) side view and electro-optic chromophore.

The photoresist coated on the Au seed layer was patterned using a photomask in a mask aligner for the Au electroplating.

A sol-gel solution consisting of methacryloyloxy propyltrimethoxysilane (MAPTMS) and an index modifier (zirconium(IV)-*n*-propoxide) at a molar ratio of 95(MAPTMS)/5 mol% was prepared for the lower-cladding, side-cladding, and upper-cladding layers of the sol-gel waveguide. A 0.1 N HCl solution was added to the sol-gel solution as a catalyst to partially hydrolyze the sol-gel solution. Irgacure 184 (Ciba) was added to the side-cladding solution as a photoinitiator for the subsequent patterning of the cladding by UV irradiation through a photomask and wet etching in isopropanol.

A 4- $\mu\text{m}$ -thick lower-cladding layer was coated on the RF electrode/substrate. The claddings were baked at 150 °C for 1 h to construct a cross-linked silica network in the lower-cladding layer. The side-cladding solution was coated on the lower-cladding layer, which was UV irradiated through a photomask in a mask aligner to pattern the waveguide structure of the side-cladding layer. The sample was wet-etched in isopropanol to remove the MZ waveguide core region and then baked at 150 °C for 1 h. A 1.7- $\mu\text{m}$ -thick guest-host EO polymer (SEO100) [33] with 35 wt% dipolar phenyltetraene chromophore doping in amorphous polycarbonate (APC) was spin-coated between the side-cladding layer on top of the lower-cladding layer and baked overnight at 80 °C in a vacuum oven. The sol-gel solution was coated on the EO polymer as an upper-cladding layer and baked

at 150 °C for 1 h. A via-hole was dry-etched on the waveguide to access the Au lower ground electrode. An Au via-pillar was fabricated using the Au electroplating technique, so that its height corresponded to the height of the waveguide and it reached the surface of the waveguide, as shown in Fig. 1. The Au seed layer was sputtered on the total surface connected with the via-pillar. The Au electroplating and liftoff technique was used to pattern the photoresist on the Au seed layer to fabricate the top Au high-speed electrode. The photoresist was removed after the Au electroplating, and the MZ waveguide modulator sample was diced for butt coupling of an optical fiber.

The EO polymer was poled between the top RF electrode and the lower ground electrode. The distance between the RF microstrip line at the RF input and top pad for the ground was 50  $\mu\text{m}$ , which is large enough for dielectric breakdown to occur during poling of the EO polymer. A poling voltage of 300 V for an inter-electrode distance ( $d$ ) of 13.3  $\mu\text{m}$  was applied at a temperature of 155 °C in a  $\text{N}_2$  environment to the EO polymer, which was then cooled to room temperature to fix the chromophore in the host polymer.

### III. DESIGN AND EXPERIMENTAL RESULT

#### A. Electrical Properties of the Modulators

We accurately measured the dielectric constant and electrical conductivity for each material and compared the value of the dielectric constant with the calculated results using the S parameter experimentally obtained using a VNA in a frequency range of 10 to 50 GHz. The measured relative dielectric constants of the EO polymer (SEO100), sol-gel silica,  $\text{SiO}_2$ , and Si were 3, 4, 4, and 11.9, respectively. The dissipation factors ( $\tan\delta$ ) of the dielectric constant of the EO polymer and sol-gel silica were 0.03 and 0.02, respectively. These values were experimentally obtained from the measurement of the phase ( $\Delta\phi_{s21}$ ) of the transmission parameter  $S_{21}$  for each thin film [34],

$$\Delta\phi_{s21} = 2\pi \sqrt{\epsilon_{eff}} f L / c \quad (1)$$

where  $f$  and  $\epsilon_{eff}$  denote the transmission signal frequency and effective dielectric constant, respectively. A 6- $\mu\text{m}$ -thick coplanar electrode of the ground-signal-ground planes (GSG) was patterned on each 1- $\mu\text{m}$ -thick EO polymer film, and a 4- $\mu\text{m}$ -thick sol-gel silica film was deposited on a 6- $\mu\text{m}$ -thick  $\text{SiO}_2/\text{Si}$  substrate to measure the dielectric constant of each material. The same coplanar electrode was also fabricated on a sapphire substrate to measure the dielectric dispersion and to validate the measurement accuracy. The experimentally obtained result for the dielectric constant of sapphire was 10.8, which was similar to the already known physical constant of 11.9, thereby validating the accuracy of the dielectric constant measurement. Following the phase of the transmission parameter  $S_{21}$  and the measurement of an insertion loss, the experimental result was curve-fitted using a three-dimensional microwave simulator known as the high-frequency electromagnetic field simulation software. The fitting result indicated that the dielectric dispersion ranged from 10 GHz to 50 GHz. The dielectric relaxation for each layer was not measured from 10 GHz to 50 GHz, which corresponded to the upper limit of the VNA (Keysight N5245A).

The dielectric dispersion for each material in the modulator was small enough to obtain wide bandwidth for the electrical transmission in the frequency range. The conductivities of the sol-gel silica, Au, and Si were  $10^{-8}$ ,  $2.2 \times 10^7$ , and  $0.1$  S/m, respectively. The conductivities of the EO polymer and  $\text{SiO}_2$  were negligible compared to those of the other materials.

EO polymers have a thirty-times-lower refractive index dispersion ( $<0.1$ ) than  $\text{LiNbO}_3$  (e.g., 3.1), which indicated a wider optical modulation bandwidth. In an optical modulator with a traveling-wave electrode, the bandwidth of the optical modulation is limited by (i) the difference between the phase velocity of the optical wave and the millimeter wave (walk-off), (ii) the characteristic impedance of the electrode, and (iii) the propagation loss of the electrode. As long as the bandwidth due to walk-off is larger than the bandwidth of the electrical transmission  $S_{21}$  and the RF transmission loss is small enough, the bandwidth of the optical modulation is same as that of the electrical transmission  $S_{21}$ . Because we used active materials with low refractive index dispersion, such as EO polymers, we can theoretically increase the RF transmission bandwidth up to the walk-off bandwidth. The product of the 3-dB bandwidth for the optical response  $\Delta f_m$  and RF electrode length  $L$  of a Pockels modulator composed of dielectric materials depends on the refractive index dispersion between the optical and millimeter frequencies without considering the electrical transmission loss and impedance mismatch:

$$\Delta f_m L = \frac{\sqrt{2}c}{\pi |n_{opt} - n_{mw}|} \quad (2)$$

where  $L$ ,  $n_{opt}(= \sqrt{\epsilon_{opt}})$ , and  $n_{mw}(= \sqrt{\epsilon_{mw}})$  denote the RF electrode length, an effective refractive index at the optical frequency, and an effective refractive index at the millimeter frequency, respectively.

We calculated the effective refractive index  $n_{opt}$  to be 1.661 for the hybrid EO polymer/sol-gel modulator from the measured refractive index of the EO polymer of 1.704 and that of the sol-gel silica of 1.487 using the 3D finite-differential time-domain (FDTD) method, which corresponds to an effective dielectric constant  $\epsilon_{opt}$  of 2.76. The product of the bandwidth and RF electrode length ( $\Delta f_m L$ ) was calculated with respect to the effective dielectric constant  $\epsilon_{mw}$  at the millimeter frequency and is shown in Fig. 2. This is helpful to see how the effective dielectric constant  $\epsilon_{mw}$  at the millimeter frequency can decide the bandwidth of the optical response due to the phase velocity mismatch when the electrical transmission loss and impedance mismatch is ignored. The optical modulator consists of the optical waveguide, where the optical wave and the millimeter interact. The optical waveguide has effective refractive index  $n_{opt}$  at the optical frequency. The phase velocity of the optical wave in the optical waveguide is delayed by the effective refractive index  $n_{opt}$ . Similarly, the optical waveguide has effective refractive index  $n_{mw}$  at the millimeter frequency.

Therefore, when the effective dielectric constant  $\epsilon_{mw}$  for the millimeter frequency of the hybrid waveguide for a desired RF frequency approaches the effective dielectric constant  $\epsilon_{opt}$  of 2.76 for the optical frequency, the product of the bandwidth and

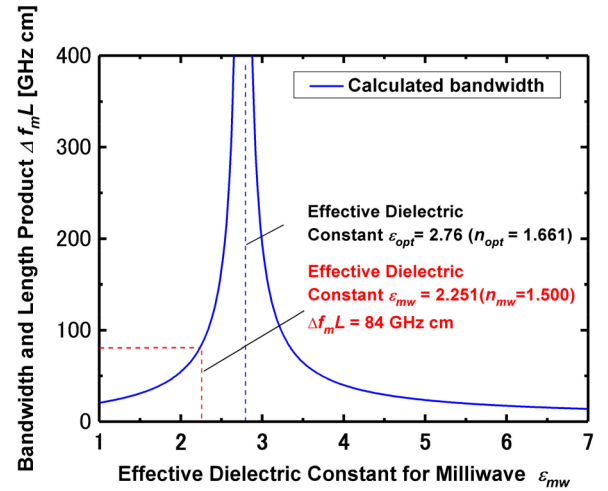


Fig. 2. Dependence of the calculated product of the bandwidth and electrode length ( $\Delta f_m L$ ) on the effective dielectric constant for the millimeter wave ( $\epsilon_{mw}$ ) due to the phase velocity mismatch between the optical wave and RF traveling wave in the modulator.

TABLE I  
CALCULATED BANDWIDTH DUE TO THE ELECTRICAL TRANSMISSION AND PHASE VELOCITY MISMATCH

RF electrode length	5 mm	10 mm
Bandwidth of RF transmission $S_{21}$	128 GHz	60 GHz
Bandwidth due to phase velocity mismatch	168GHz	84 GHz

RF electrode length will further increase. The effective dielectric constant  $\epsilon_{mw}$  at the millimeter frequency was calculated to 2.251 based on the experimentally obtained dielectric constant and conductivity using Ansys high frequency simulation software (HFSS) after the optimization of the optical waveguide structure. The product of the bandwidth and electrode length  $\Delta f_m L$  due to walk-off was calculated to be 84 GHz cm. The bandwidth of the phase velocity mismatch and the electrical transmission for each RF electrode are given in Table I.

Because the RF transmission bandwidth is narrower than that of the phase velocity mismatch, the bandwidth of the experimentally obtained electrical transmission  $S_{21}$  corresponds to that of the optical modulation. Therefore, the RF transmission bandwidth, which indicates the optimization of the impedance matching and reduction of the propagation loss of the electrode, is an important parameter to measure. The broadband frequency response of the modulator was demonstrated by measuring the electrical transmission  $S_{21}$  parameter on two RF VNAs (Keysight N5245A and Anritsu ME7808). The input and output of the modulator were connected using millimeter probes through a millimeter cable, and the output probe was terminated.  $S_{21}$  was measured from a low frequency of 10 MHz to a high frequency of 110 GHz, which was divided into two bandwidths, 10 MHz to 50 GHz (Keysight N5245) and 65 GHz to 110 GHz (Anritsu ME7808).  $S_{21}$  at 0 dB was set to 40 MHz for the measurement from 65 GHz to 110 GHz.

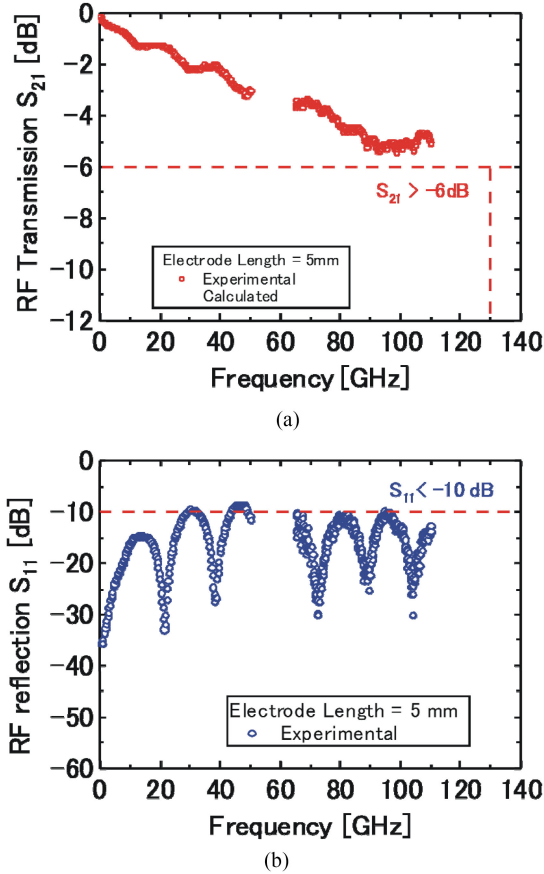


Fig. 3. Frequency response of (a) the RF transmission parameters  $S_{21}$  and (b) the RF reflection parameters  $S_{11}$ , for the broadband hybrid EO polymer/sol-gel silica waveguide modulator. Red and blue dots indicate the experimental results for the modulators with 5-mm-long RF electrodes.

The experimentally obtained response of the electrical transmission parameter  $S_{21}$  for a 5-mm-long single-drive modulator can be well explained by the theoretically calculated parameters shown in Fig. 3.  $S_{21}$  was reduced by 4.6 dB at the VNA limit of 110 GHz, which led to a bandwidth of 130 GHz for a 6-dB decrease in the transmission parameter  $S_{21}$ , which corresponded to the bandwidth of the EO response for a 3-dB decrease in the transmission parameter, as the VNA detects optical power as the power source and electrical signals as the amplitude. The top RF microstrip line electrode was designed to achieve phase velocity matching between the optical wave and milliwave while maintaining an impedance matching of 50  $\Omega$ . The electrical reflection  $S_{11}$  was also measured and is shown in Fig. 3(b).  $S_{11}$  was less than  $-10$  dB over the measured frequency range from 10 MHz to 110 GHz, which also ensured impedance matching. The value of  $d$  (13.3  $\mu\text{m}$ ) that corresponded to the total thickness of the sol-gel silica cladding and the EO polymer in conjunction with the 6- $\mu\text{m}$ -thick top RF electrode increased the bandwidth to a maximum of 130 GHz.

The calculation result for  $S_{21}$  indicated that all significant decreases reached a maximum of 130 GHz, which corresponded to the widest bandwidth compared to all other non-Pockels InP modulators (e.g., approximately 74 GHz) [13] and LiNbO<sub>3</sub> modulators [16], [17]. The experimental results indicated that the

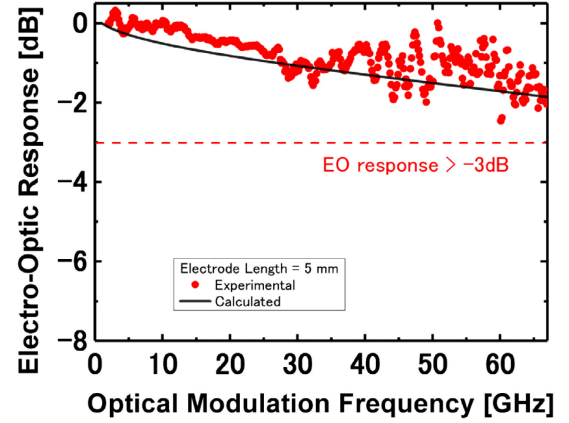


Fig. 4. Frequency response of EO modulation for the broadband hybrid EO polymer/sol-gel silica waveguide modulator. The red circles indicate the experimental results for the modulators with 5-mm-long RF electrodes. The black line indicates the calculated results. The LCA had a frequency limitation of 67 GHz.

input impedance of 50  $\Omega$  at the input port was widely matched to the impedance by the proposed modulator design.

### B. Electro-Optic Response

Furthermore, the EO response (EO modulation index) of the modulator was measured up to the highest frequency of 67 GHz using an LCA (Keysight 81960A), which is the upper limit of frequency of commercially available LCAs. The optical and RF input power was 40 mW at a wavelength of 1550 nm and 0 dBm (0.224 V at 50  $\Omega$  load), respectively. The measured result for the modulator with a 5-mm-long RF electrode showed a 1.5-dB reduction in the optical response for an EO-modulated frequency of 67 GHz, as shown in Fig. 4, which also indicates an extrapolated 3-dB bandwidth for the EO response of  $>100$  GHz from the theoretical result.

An RF probe (Cascade Microtech APC65-GSG-250) and RF cable (Cascade Microtech 145-605-B) with upper frequency limits of 65 and 67 GHz, respectively, were used for the LCA measurement. This limitation results in noisy high-frequency LCA measurements near the upper limit. When the characteristic impedance of the RF traveling wave in the microstrip line electrode is matched the driver and the load, considering the electrical loss, the EO response  $M(f)$  can be expressed as a function of the optical modulation frequency [35].

$$M(f) = e^{-\alpha L/2} \left| \frac{\sinh^2(\alpha L/2) + \sin^2(\xi L/2)}{(\alpha L/2)^2 + (\xi L/2)^2} \right| \quad (3)$$

where

$$\xi = 2\pi f |n_{mw} - n_{opt}| / c \quad (4)$$

where  $\alpha$  is the attenuation constant of the RF traveling wave. The calculated EO response was fitted with the experimentally obtained response for the modulator with a 5-mm-long RF electrode. Our result for the optical modulation bandwidth with a 5-mm-long RF electrode showed less reduction in the optical modulation up to 67 GHz and a wider optical bandwidth than that of previously reported polymer MZ modulators [36]. These

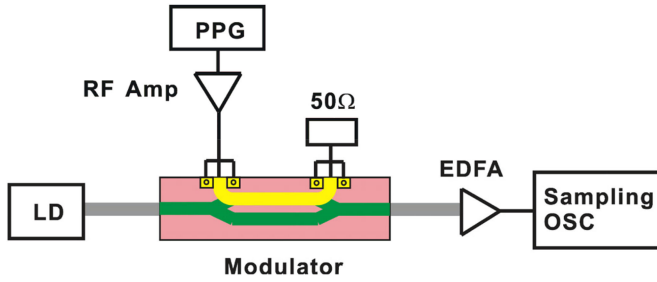


Fig. 5. Experimental setup to examine the eye diagram of the EO response of a single-drive modulator using a 56-Gbps programmable PPG and a sampling oscilloscope. LD: distributed feedback laser diode. EDFA: erbium-doped fiber amplifier. The measurement equipment had a bandwidth limitation of 40 GHz.

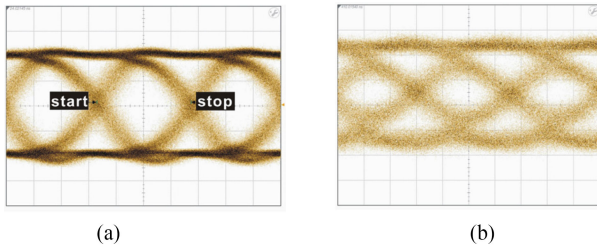


Fig. 6. The eye diagrams of (a) the electrical input to the EO modulator and (b) the optical output from the EO modulators (single-drive operation and 5-mm-long RF electrode) measured on the sampling oscilloscope at 56 Gbps. The limited bandwidth of the electronic equipment of 40 GHz resulted in the sinusoidal shape of the eye diagram. Time scale: 5 ps/div.

results corresponded to the widest bandwidth compared to all other non-Pockels InP modulators (e.g., extrapolated to 74 GHz) [13] and LiNbO<sub>3</sub> modulators [16], [17].

### C. Measurements of the Eye Diagram

An eye diagram at the EO modulation speed of 56 Gbps was measured for the optical modulators, as shown in Fig. 5, using a pseudorandom binary sequence pulse pattern generator (Keysight N4975A) and a sampling oscilloscope (Keysight 86100D). The output optical signal was amplified using an erbium-doped fiber amplifier (EDFA) to accurately measure the eye diagram on the sampling oscilloscope. The probes used in the experiments were the same as those used in the small signal modulation experiments to measure the electrical transmission  $S_{21}$ . The signal from a pulse pattern generator (PPG) was RF amplified to the level of  $V_{\pi}$  and placed into the modulator using a milliwave probe, as shown in Fig. 5. The output pulse was coupled out using another probe and terminated by a 50- $\Omega$  terminator connected to the probe. A distributed feedback laser at 1.55  $\mu\text{m}$  was coupled to the modulator using a tapered single-mode fiber. The output light was coupled out using another tapered fiber, following modulation (non-return-zero signal) by the PPG. The output light was amplified on the EDFA to compensate for the fiber-to-fiber coupling. The amplified optical signal was placed into the sampling oscilloscope to measure the eye diagram.

The eye diagrams measured on the sampling oscilloscope at 56 Gbps are shown in Fig. 6. The electrical equipment used to

measure the eye diagram had a bandwidth of 40 GHz, which resulted in a sinusoidal shape for the input RF signal, instead of a rectangular shape, as shown in Fig. 6(a). The eye diagram for the optical output showed a similar shape to the electrical eye diagram with an extinction ratio of 2.25 dB, as shown in Fig. 6(b). This measurement ensured that the optical eye diagram followed the electrical eye diagram. It is not suitable to compare the result of the optical eye diagram with the result based on measurements using electrical equipment with a wider bandwidth.

Moreover, the eye diagrams of the push-pull dual-drive modulators were also examined to reduce the driving voltage, using a 10-mm-long RF electrode fabricated on both optical waveguide branches of the MZ modulators. The PPG signal was separated and amplified using an RF amplifier (AH54147A, Anritsu) for both RF electrodes of the dual-drive modulator. The electrical phase of each pulse was adjusted to different polarities using electrical delay lines (A60V, Waka Manufacturing Co.) to obtain push-pull operation. The output of each RF electrode was terminated using 50  $\Omega$  impedance loads. “A pulsed peak-to-peak voltage of 1.5–3.0 V was applied to the modulator during the eye diagram measurement with the extinction ratio of 3.93–6.88 dB. When the pulsed peak-to-peak voltage is increased to 8 V, the extinction ratio was 7.11 dB. Even though the pulse voltage was reduced to 1.5 V and the equipment used to obtain the eye diagram had a limited bandwidth of 40 GHz, the eye diagram was obtained at 56 Gbps on the sampling oscilloscope. The measurement of the bandwidth and the eye diagram indicated that the modulator exhibited considerably higher speed modulation (e.g., >100 Gbps).

### D. Half-Wave Voltage of the Modulators

The  $V_{\pi}$  at 1550 nm was measured for the hybrid EO polymer/sol-gel silica waveguide modulator with a 5-mm-long RF electrode, which indicated a bandwidth of 130 GHz. The input light was controlled for the polarization state excited by a transverse magnetic mode in the modulators using a polarization controller. The optical output of the output fiber was placed into an optical detector. A time-varying voltage with a triangular waveform was applied between the RF top milliwave electrode and lower ground electrode at a frequency of 10 kHz. The voltage was applied to a single MZ waveguide for single-drive operation. The intensity-modulated output from the MZ modulator detected by an optical detector was monitored on an oscilloscope along with the voltage signal. Additionally,  $V_{\pi}$  was measured for the modulators at a wavelength of 1550 nm based on the transfer function between the voltage signal and the optical signal, as shown in Fig. 7.

A  $V_{\pi}L$  value for the hybrid modulator with a 5-mm-long RF electrode was 4.15 V-cm (single drive) at 10 kHz. A  $V_{\pi}L$  value of 1.8 V-cm was also obtained for the 10-mm-long RF electrode (Fig. 7) when both RF electrodes of the broadband hybrid modulator were poled and driven in a dual-drive operation. The difference in  $V_{\pi}L$  values was derived from the poling efficiency of each modulator. The in-device EO coefficient was found to be 160 pm/V from  $V_{\pi}L = 0.8 \text{ V-cm}$ ,  $d = 13.3 \mu\text{m}$ , and a mode overlap integral of 0.73. The mode overlap integral

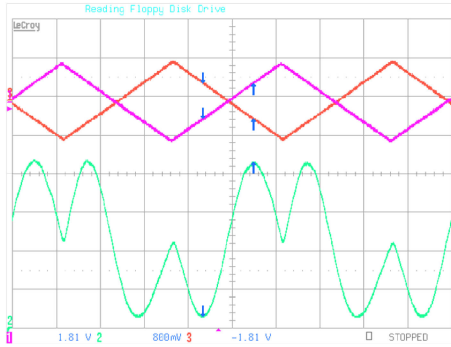


Fig. 7. Half-wave voltage  $V_\pi$  measured for the ultra-broadband modulator under dual-drive operation at 10 kHz.  $V_\pi L = 1.8$  V-cm ( $d = 13.3$   $\mu\text{m}$ ,  $L_e = 10$  mm) at 1550 nm.

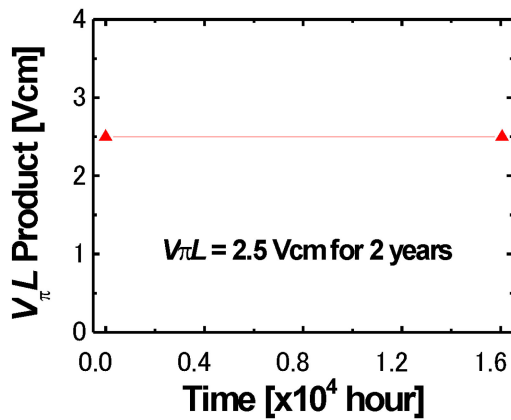


Fig. 8. Long-term stability of the half-wave voltage ( $V_\pi$ ) measured for a modulator at 1 kHz.  $V_\pi L = 2.5$  V-cm at 1550 nm.

was calculated from a perfectly fabricated waveguide, using the 3D FDTD method. Therefore, the actual mode overlap integral is less than 0.73, and the in-device EO coefficient is more than 160 pm/V.

A previously fabricated hybrid modulator for the  $V_\pi$  measurement of similar guest-host EO polymers was examined to determine the long-term stability over two years. The samples were kept at random variations of room temperature to a maximum of 40 °C in air without any protection. The  $V_\pi L$  value of 2.5 V-cm did not change over two years, as shown in Fig. 8, which indicated that the hybrid modulator was stable for long-term usage when the modulator was used in temperature-controlled conditions.

### E. Optimized Design for Wider Bandwidths of More Than 140 GHz

The electrical transmission parameters of the modulators with 2.5-, 5-, and 10-mm-long RF electrodes were calculated with the same device parameters using HFSS and considering the impedance mismatch, as shown in Fig. 9.

The bandwidth of 6-dB reduction (which corresponds to a bandwidth of 3-dB reduction for the EO response) was more than 140 GHz for the modulator with the 2.5-mm-long RF electrode. However, when we consider the frequency of 140 GHz,

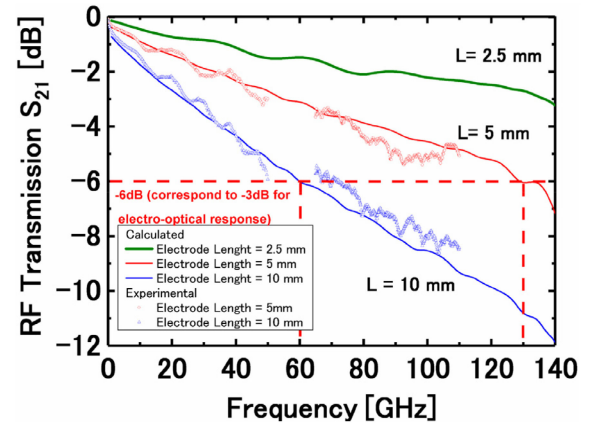


Fig. 9. Frequency response of the electrical transmission for the modulators. The green, red and blue lines indicate the calculated results for the modulators with 2.5-, 5-, 10-mm-long RF electrodes, respectively. The calculated results were considered for the electrode loss and impedance mismatch, using Ansys HFSS software. The red circles and blue triangles indicate the experimental results for the modulators with 5- and 10-mm-long RF electrodes, respectively.

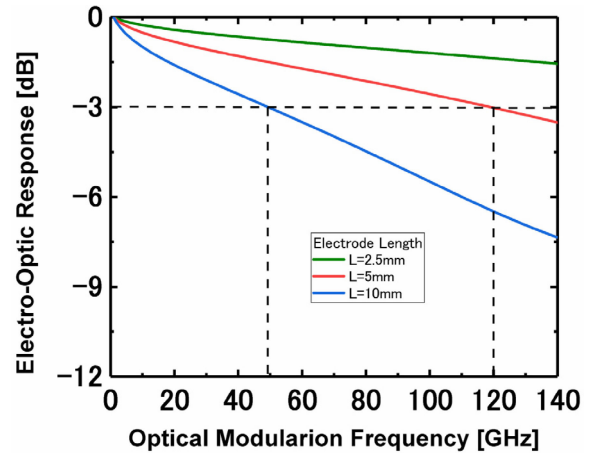


Fig. 10. Calculated frequency response of the EO response for the modulators when the electrode loss was considered and the impedance is completely matched. The green, red and blue lines indicate the results for the modulators with 2.5-, 5-, 10-mm-long RF electrodes, respectively.

we can assume reduction of 3 dB for the electrical transmission  $S_{21}$  as shown in Fig. 9. Therefore, the  $V_\pi$  will be increased to 10.18 V ( $=7.2$  V/0.707) for 2.5-mm-long RF electrode, which can be calculated the driving voltage of 7.4 V to maintain extinction ratio of 7 dB at the modulation frequency of 140 GHz. We may need a RF power amplifier or reduce the  $V_\pi$  further. The RF transmission for the modulator with the 10-mm-long RF electrode was also experimentally measured to ensure that the calculation based on HFSS is valid when the same device parameters are used. The bandwidth of the electrical transmission for the modulators with 5 and 10-mm-long RF electrodes was calculated to be 130 and 60 GHz, respectively. The experimentally obtained transmission  $S_{21}$  parameter matched the calculated parameter within a maximum error range of 0.5 dB to a frequency of 50 GHz based on the measured parameters. This implied that the refractive index dispersion of the EO polymer enabled a wider bandwidth exceeding 130 GHz for MZ

modulators when an electrode less than 2.5 mm in length was used, as opposed to the aforementioned demonstration using a 5-mm-long electrode. There was no dipping in the electrical transmission parameter  $S_{21}$  experimentally and theoretically from the frequency with respect to MHz to 110 GHz as shown in Fig. 9, which also proved that our measured dielectric constants were accurate and the dispersion was small enough in the frequency range of 10 to 50 GHz. The EO response with respect to the optical modulation frequency for the modulators with 2.5-, 5-, and 10-mm-long RF electrodes was calculated, as shown in Fig. 10, based on eq. (3) using the same device parameters obtained from the measurement of the EO response for the modulator with the 5-mm-long RF electrode, as shown in Fig. 4.

The 3-dB bandwidth of the EO response for the modulators with 5- and 10-mm-long RF electrodes was 120 and 50 GHz, respectively. The bandwidth for the EO response was calculated to be narrower than that of the RF transmission by 10 GHz for each RF electrode length.

#### IV. CONCLUSION

Optical modulators, such as Si, LiNbO<sub>3</sub>, InP, all-polymer, EO polymer/Si slot, and EO polymer/Au plasmon modulators, do not show bandwidths over 67 GHz (3-dB reduction) via LCA measurement. We compared the bandwidth from the reduction in the optical modulation at a frequency of 67 GHz by using a commercially available LCA. We accurately measured the dielectric constant, the conductivity and the dissipation factor ( $\tan\delta$ ) of each material based on our technique and obtained an optical modulation bandwidth  $\Delta f_m L = 84$  GHz cm, considering the phase velocity mismatch. The phase velocity mismatch mainly results from the refractive index dispersion of the active materials, the RF impedance mismatch (50  $\Omega$ ) and the RF electrode loss due to errors in the electrode design and fabrication. The EO polymer had a low refractive index dispersion of  $<0.1$ , which was 30 times lower than that of LiNbO<sub>3</sub> (3.1). The optical bandwidth of the polymer modulators can be maximized when the design and fabrication of the RF electrode is optimized from the accurately measured dielectric constant and conductivity, which we examined extensively. The results indicated great potential for the hybrid modulators when the RF electrode length was further reduced and optimized, which enables an increased bandwidth. The optimization of the electrode design and fabrication for these modulators was ensured for the electrical transmission  $S_{21}$  parameter by using a VNA.

This study involved the measurement of the bandwidth of broadband EO polymer/sol-gel silica waveguide modulators to a maximum value of 110 GHz, which was extrapolated to 130 GHz from the experimentally measured parameters. The initial measurement of the optical eye diagram corresponded to 56 Gbps, even though the measurement equipment had a bandwidth limitation of 40 GHz. When electronics with wider bandwidths are available, the optical eye diagram can be measured over a wider range. The measured response for the EO modulation at a frequency of 67 GHz for the modulator with 5-mm-long RF electrode indicated the bandwidth of 120 GHz, which can

demonstrate the bit rate of 160 Gbps. The EO polymer was efficiently poled with respect to the broadband modulators, and the in-device EO coefficient was more than 160 pm/V at 1.55  $\mu\text{m}$ . A  $V_\pi L$  value of 1.8 V-cm was measured for the dual-drive broadband hybrid modulator, and the propagation loss corresponded to 6 dB/cm. The measured  $V_\pi L_{\text{loss}}$  value of 10.8 V-cm is the lowest value among ultra-broadband modulators [12].

#### REFERENCES

- [1] S. Masuda, A. Seki, K. Shiota, H. Hara, and Y. Masuda, "Electro-optic and dielectric characterization of ferroelectric films for high-speed optical waveguide modulators," *J. Appl. Phys.*, vol. 109, no. 12, Jun. 2011, Art. no. 124108.
- [2] S. Abe, S. Masuda, K. Uekusa, H. Hara, and M. Shimizu, "Photonics integrated circuit using lanthanum-modified lead zirconate titanate thin film," in *Proc. Conf. Opt. Fiber Commun.*, 2017, Paper Th31.2.
- [3] N. Feng *et al.*, "High speed carrier-depletion modulators with 1.4 V-cm  $V_\pi L$  integrated on 0.25  $\mu\text{m}$  silicon-on-insulator waveguides," *Opt. Express*, vol. 18, no. 8, pp. 7994–7999, Apr. 2010.
- [4] H. Xu *et al.*, "High-speed silicon modulator with band equalization," *Opt. Lett.*, vol. 39, no. 16, pp. 4839–4842, Aug. 2014.
- [5] D. Petousi *et al.*, "Analysis of optical and electrical tradeoffs of traveling-wave depletion-type Si Mach-Zehnder modulators for high-speed operation," *IEEE J. Sel. Topics Quantum Electron.*, vol. 21, no. 4, Jul./Aug. 2015, Art. no. 3400108.
- [6] L. Yang and J. Ding, "High-speed silicon Mach-Zehnder optical modulator with large optical bandwidth," *J. Lightw. Technol.*, vol. 32, no. 5, pp. 966–970, Mar. 2014.
- [7] D. Thomson *et al.*, "50-Gb/s silicon optical modulator," *IEEE Photon. Technol. Lett.*, vol. 24, no. 4, pp. 234–236, Feb. 2012.
- [8] H. Xu *et al.*, "High-speed silicon modulator with band equalization," *Opt. Lett.*, vol. 39, no. 16, pp. 4839–4842, Aug. 2014.
- [9] M. Ziebell *et al.*, "40 Gbit/s low-loss silicon optical modulator based on a p-i-n diode," *Opt. Express*, vol. 20, no. 10, pp. 10591–10596, May 2012.
- [10] I. Goykhman, B. Desiatov, S. Ben-Ezra, J. Shappir, and U. Levy, "Optimization of efficiency-loss figure of merit in carrier-depletion silicon Mach-Zehnder optical modulator," *Opt. Express*, vol. 21, no. 17, pp. 19518–19529, Aug. 2013.
- [11] M. Watts, W. Zortman, D. Trotter, R. Young, and A. Lentine, "Low-voltage, compact, depletion-mode, silicon Mach-Zehnder modulator," *IEEE J. Sel. Topics Quantum Electron.*, vol. 16, no. 1, pp. 159–164, Jan./Feb. 2010.
- [12] Y. Enami, H. Nakamura, J. Luo, and A. K. Y. Jen, "Analysis of efficiently poled electro-optic polymer/TiO<sub>2</sub> vertical slot waveguide modulators," *Opt. Commun.*, vol. 362, pp. 77–80, Mar. 2016.
- [13] Y. Tang, J. Peters, and J. Bowers, "Over 67 GHz bandwidth hybrid silicon electroabsorption modulator with asymmetric segmented electrode for 1.3  $\mu\text{m}$  transmission," *Opt. Express*, vol. 20, no. 10, pp. 11529–11535, May 2012.
- [14] Y. Ogiso *et al.*, "100 Gb/s and 2 V V InP Mach-Zehnder modulator with an n-i-p-n heterostructure," *Electron. Lett.*, vol. 52, no. 22, pp. 1866–1867, Oct. 2016.
- [15] E. Wooten *et al.*, "A review of lithium niobate modulators for fiber-optic communications systems," *IEEE J. Sel. Topics Quantum Electron.*, vol. 6, no. 1, pp. 69–82, Jan./Feb. 2000.
- [16] A. Mercante, P. Yao, S. Y. Shi, G. Schneider, J. Murakowski, and D. Prather, "110 GHz CMOS compatible thin film LiNbO<sub>3</sub> modulator on silicon," *Opt. Express*, vol. 24, no. 14, pp. 15590–15595, Jul. 2016.
- [17] J. Macario *et al.*, "Full spectrum millimeter-wave modulation," *Opt. Express*, vol. 20, no. 21, pp. 23623–23629, Oct. 2012.
- [18] K. Noguchi, O. Mitomi, and H. Miyazawa, "Millimeter-wave Ti: LiNbO<sub>3</sub> optical modulators," *J. Lightw. Technol.*, vol. 16, no. 4, pp. 615–619, Apr. 1998.
- [19] T. Kawanishi, K. Kogo, S. Oikawa, and M. Izutsu, "Direct measurement of chirp parameters of high-speed Mach-Zehnder-type optical modulators," *Opt. Commun.*, vol. 195, nos. 5–6, pp. 399–404, Aug. 2001.
- [20] Y. Shi, L. Yan, and A. Willner, "High-speed electrooptic modulator characterization using optical spectrum analysis," *J. Lightw. Technol.*, vol. 21, no. 10, pp. 2358–2367, Oct. 2003.
- [21] C. Hoessbacher *et al.*, "Plasmonic modulator with >170 GHz bandwidth demonstrated at 100 GBd NRZ," *Opt. Express*, vol. 25, no. 3, pp. 1762–1768, Feb. 2017.



- [22] Y. Enami *et al.*, "Hybrid polymer/sol-gel waveguide modulators with exceptionally large electro-optic coefficients," *Nature Photon.*, vol. 1, no. 3, pp. 180–185, Mar. 2007.
- [23] Y. Enami *et al.*, "Hybrid cross-linkable polymer/sol-gel waveguide modulators with 0.65 V half wave voltage at 1550 nm," *Appl. Phys. Lett.*, vol. 91, no. 9, Aug. 2007, Art. no. 093505.
- [24] Y. Enami, A. Seki, S. Masuda, J. Luo, and A. Jen, "Ultra-broadband Mach-Zehnder hybrid electro-optic polymer/sol-gel silica waveguide modulators," in *Proc. Conf. Lasers Electro-Opt.*, 2017, Paper SM2O.5.
- [25] D. Chen *et al.*, "Demonstration of 110 GHz electro-optic polymer modulators," *Appl. Phys. Lett.*, vol. 70, no. 25, pp. 3335–3337, Jun. 1997.
- [26] H. Huang *et al.*, "Broadband modulation performance of 100-GHz EO polymer MZMs," *J. Lightw. Technol.*, vol. 30, no. 23, pp. 3647–3652, Dec. 2012.
- [27] T. Baehr-Jones *et al.*, "Ultralow drive voltage silicon traveling-wave modulator," *Opt. Express*, vol. 20, no. 11, pp. 12014–12020, May 2012.
- [28] L. Alloatti *et al.*, "100 GHz silicon-organic hybrid modulator," *Light-Sci. Appl.*, vol. 3, May 2014, Art. no. e173.
- [29] S. Koeber *et al.*, "Femtojoule electro-optic modulation using a silicon-organic hybrid device," *Light-Sci. Appl.*, vol. 4, Feb. 2015, Art. no. e255.
- [30] Y. Enami, B. Yuan, M. Tanaka, J. Luo, and A. Jen, "Electro-optic polymer/TiO<sub>2</sub> multilayer slot waveguide modulators," *Appl. Phys. Lett.*, vol. 101, no. 12, Sep. 2012, Art. no. 123509.
- [31] Y. Enami, Y. Jouane, J. Luo, and A. Jen, "Enhanced conductivity of sol-gel silica cladding for efficient poling in electro-optic polymer/TiO<sub>2</sub> vertical slot waveguide modulators," *Opt. Express*, vol. 22, no. 24, pp. 30191–30199, Dec. 2014.
- [32] D. Zhang and Y. Enami, "Simulation for optical response of high speed traveling wave electro-optic polymer/TiO<sub>2</sub> multilayer slot waveguide modulators," *IEEE Photon. J.*, vol. 9, no. 3, Jun. 2017, Art. no. 5501809.
- [33] Y. Jouane, Y. Chang, D. Zhang, J. Luo, A. Jen, and Y. Enami, "Unprecedented highest electro-optic coefficient of 226 pm/V for electro-optic polymer/TiO<sub>2</sub> multilayer slot waveguide modulators," *Opt. Express*, vol. 22, no. 22, pp. 27725–27732, Nov. 2014.
- [34] H. Lue, and T. Tseng, "Application of on-wafer TRL calibration on the measurement of microwave properties of Ba<sub>0.5</sub>Sr<sub>0.5</sub>TiO<sub>3</sub> thin films," *IEEE Trans. Ultrason., Ferroelectr., Freq. Control*, vol. 48, no. 6, pp. 1640–1647, Nov. 2001.
- [35] N. Dagli, "Wider bandwidth lasers and modulators for RF photonics," *IEEE Trans. Microw. Theory Techn.* vol. 47, no. 7, pp. 1151–1171, Jul. 1999.
- [36] J. Mallari *et al.*, "100 Gbps EO polymer modulator product and its characterization using a real-time digitizer," in *Proc. Conf. Opt. Fiber Commun.*, 2010, Paper OthU2.

Authors' biographies not available at the time of publication.